Design and Implementation of Multi-variable H∞ Robust Control for the Underground Coal Gasification Project Thar

Article *in* Energy · October 2020

DOI: 10.1016/j.energy.2020.119000

CITATIONS
8

READS
108

4 authors:

Syed Bilal Javed
National Engineering & Scientific Commission, Islamabad, Pakistan
11 PUBLICATIONS **47** CITATIONS
SEE PROFILE

Ali Arshad
COMSATS University Islamabad
39 PUBLICATIONS **364** CITATIONS
SEE PROFILE

Raza Samar
Capital University of Science & Technology
71 PUBLICATIONS **1,419** CITATIONS
SEE PROFILE

Aamer Iqbal Bhatti
University of Engineering & Technology Lahore
245 PUBLICATIONS **2,091** CITATIONS
SEE PROFILE

Design and Implementation of Multi-variable H_∞ Robust Control for the Underground Coal Gasification Project Thar

Syed Bilal Javed[a,b,*], Ali Arshad Uppal[b], Raza Samar[a], Aamer Iqbal Bhatti[a]

[a] *Department of Electrical Engineering, Capital University of Science and Technology, Islamabad, Pakistan*

[b] *Department of Electrical and Computer Engineering, COMSATS University Islamabad, Islamabad, Pakistan*

Abstract

The energy per unit time is an important performance indicator in determining the performance of an underground coal gasification (UCG) site to produce electricity. In literature, model-based strategies are employed by considering UCG as a single input single output (SISO) system, in which only the heating value of syngas is maintained at the desired level by varying inlet gas flow rate. However, the energy per unit time is also dependent on the flow rate of the produced gas mixture. Therefore, in this work, a model-based multi-variable robust control design, based on H_∞ technique is proposed for the UCG process. The actual nonlinear model of UCG is very complex due to its 3D axisymmetric geometry, which makes the model-based control design a formidable task. Thus, a simple linear model with two inputs (flow rate and composition of inlet gas) and two outputs (flow rate and heating value of syngas) is identified by using subspace-based (N4SID) system identification technique. The linear model is then employed to design the H_∞ (S/KS mixed sensitivity) multi-variable robust controller. The simulation results show that the designed controller has achieved both robust stability and performance in the presence of modeling inaccuracies and external disturbance. Furthermore, the designed controller is also implemented on the actual nonlinear cavity simulator (CAVSIM) for the UCG process. The controller exhibits an adequate performance by tracking the desired set

*Corresponding author: s.bilal.javed@gmail.com, syedbilal@comsats.edu.pk

points for the heating value and flow rate of the syngas.

Keywords: Underground coal gasification (UCG), Energy conversion systems, System identification, Multi-variable robust control

---

1. Introduction

Coal has become the most rapidly growing global energy fuel to produce electricity after the advent of integrated gasification combined cycle (IGCC) technology [1]. Clean coal technologies are employed to address the detrimental impact of coal combustion on both water and air quality, in which harmful gases can be removed before, during and after the combustion of coal [2–5]. Underground coal gasification (UCG) is a clean coal technology, generally applicable for low-grade, deep and un-mineable coal reserves [6, 7]. In UCG, inlet and outlet wells are drilled from surface to the coal seam, and suitable oxidants are injected through inlet well. These oxidants chemically react with coal and produce a syngas, which is collected at the outlet well [8, 9]. The quality of syngas produced by UCG process depends on the coal bed properties and operating parameters, like the composition and flow rate of inlet gas, concentration of O_2, steam to oxygen ration, temperature and pressure [10, 2]. The syngas can be used in various industrial applications, such as the ammonia, fertilizers and IGCC [11, 12].

The UCG project Thar (UPT) has been launched in Block V of Thar coal field by the planning commission of Pakistan [13–15]. The fundamental aim of this project is to develop a UCG based power plant to produce electricity at a low cost. This project has a huge significance to meet the energy demands of the country by utilizing the coal deposits located in Thar [9, 14]. In industrial applications like IGCC, the heating value and flow rate of syngas are the important performance indicators for any UCG site [16]. The only tuning knobs to attain the desired heating value and flow rate of syngas are the inlet gas flow rate and composition.

1.1. Related work

The design of UCG control system is a formidable task, as the process occurs insitu, and it involves slowly varying disturbances, uncertainties in insitu environment and lack of the direct control over the process parameters. Moreover, the installation of sensors at various locations in the UCG

reactor is in itself a challenging task [9], and thus it is impossible to measure all the essential process parameters. In the literature, UCG control system is designed by employing model-free and model-based control techniques. In [17–19], various controllers such as proportional summing (PS), bang-bang and proportional integral (PI) have been implemented for the lab scale UCG setup. The controllers are employed to control the temperature, concentrations and heating value of syngas. In [20], authors have designed an optimal controller for the similar UCG setup, in which the amount of CO was maximized. The idea of UCG control system based on lab scale setup cannot be employed on the actual UCG field [9, 21].

The model-based control technique has been used for UCG to maintain the heating value of syngas. Uppal et al. [14] have designed an equivalent control based sliding mode control [22] for the simple UCG model comprised of ordinary differential equations. The model is based on the assumption that all the states are measurable, which is not possible at the actual site. In [15], authors have proposed a sophisticated control oriented one-dimensional (1D) packed bed UCG model comprising of partial differential equations. The syngas composition and heating value are determined as a function of coal bed properties and different operating parameters. Moreover, a constrained nonlinear optimization technique is implemented to optimize three stoichiometric coefficients of coal pyrolysis reaction. In [23, 24], authors have proposed the design of super-twisting and conventional sliding mode controllers, respectively, which are based on the model of [15]. Moreover, the state measurements were not required for the implementation of controllers and the calorific value of syngas was maintained at the desired level. In [25, 26], authors have employed the simple UCG model [14] to design an integral sliding model control (ISMC) and dynamic integral sliding mode control (DISMC) for maintaining the desired heating value trajectory. A gain-scheduled modified Utkin observer has been designed to reconstruct the unknown states. It has also been shown that the proposed nonlinear control and estimation techniques exhibit robustness against parametric uncertainties, an input disturbance and measurement noise. Chaudhry et al. [21] have linearized the simple UCG model proposed by [14], and on the basis of linear model a robust multi-objective H_2/H_∞ controller is designed to keep the heating value of syngas at the desired level.

1.2. Motivation

The energy output per unit time is an important performance indicator of a UCG gasifier, which depends on the heating value and the mass flow rate of syngas [16, 27, 28]. In the literature [9, 14, 15, 21, 23–26], the closed-loop UCG system is devised by considering the UCG process as a single input single output (SISO) system. The controllers are designed to maintain the heating value of syngas at a desired level by manipulating the flow rate of inlet gas. While the flow rate of syngas has not been controlled, which has a paramount importance in determining the potential of a UCG site for electricity production. Thus, it is essential to devise a multi-variable, model-based control system for the UCG process.

The selection of a model has a significant importance in the design of model-based control technique. The capabilities of model to predict the essential process parameters and ease of control design are important factors in the selection of model, but there is always a trade off involved in it. In our previous work [29], the primary and foremost requirement was to predict the important process parameters which are not measurable at the UPT field. These process parameters include cavity growth, water influx, char production and interaction of cavity with overburden. The modeling of water influx and multidimensional cavity growth phenomena in UCG cannot be described by a simple 1D UCG models proposed by Uppal et al. [9, 14, 15, 23–26]. A 3D axisymmetric cavity simulation model (CAVSIM), developed by Lawrence Livermore National Laboratory (LLNL) USA [30], was used to predict those process parameters. For that purpose, CAVSIM was parametrized with the coal bed properties and operating conditions of Thar coal fields. The model was validated with the UPT field data by comparing the heating value and composition of the product gas. CAVSIM is an accurate, comprehensive UCG model and has already been applied to many UCG fields [31], but its complexity makes the design of model-based control a challenging task.

1.3. Major contributions

In this work, a multi-variable linear model of UCG is identified by employing a subspace-based (N4SID) system identification technique. Design of input excitation signal and acquiring of input-output data is very critical for any system identification technique. For the input design, pseudo random binary sequence (PRBS) is chosen as a test signal and designed on the basis of information gathered through preliminary experiments. The input-output data are generated by CAVSIM simulator and N4SID method in System

identification toolbox of Matlab is used to identify the linear model. The identified linear model has two inputs: flow rate and composition of inlet gas mixture and two outputs: flow rate and heating value of syngas. The model is then employed to design an H_∞ controller using S/KS mixed sensitivity method to obtain the desired values of the outputs. Moreover, the robust stability and performance of designed controllers have been shown in the presence of input disturbance and uncertainties. Finally, the H_∞ controller is implemented on the actual nonlinear model (CAVSIM). The simulation results show that the closed-loop system achieves the desired objectives.

The rest of the article is organized in the following manner. Section 2 describes the identification of linear model. The design of H_∞ multi-variable robust controller and robust stability and performance analysis are given in Section 3. In Section 4, implementation of H_∞ multi-variable robust controller on the nonlinear model is discussed, and finally the paper is concluded in Section 5.

2. System Identification

In this work, the complexity of a CAVSIM is a major limitation in the designing of a model-based controller. Thus, a simplified multi-variable linear model is developed by employing a N4SID system identification technique. The most important part of identification process is to design an input signal and acquiring input-output data, which are challenging due to the experimental and economical constraints associated with the conduction of field trials [33–35]. Thus, the identification experiments are performed on CAVSIM in order to generate the essential input-output data sets. The identified linear model based on CAVSIM preserves all the essential process dynamics, and it provides an ease to design a multi-variable control system for the UPT field. The system identification technique has been discussed in the subsequent sections.

2.1. Preliminary identification experiments

Prior to conduct the model estimation experiments, the preliminary staircase and step experiments are performed to determine the linear operating range and nonlinear plant parameters such as static gains, delays, time constants and bandwidth [33, 36, 37]. Moreover, it is pertinent to mention that the step test must be performed at least in two directions to determine the linear operating range and effects of nonlinearities.

The selection of operating point is important to identify the linear model, and it should lie within the linear range of the process. If an operating point lies on the boundary or outside of the linear operating range then large modeling errors can occur, resulting in a poor system identification [37]. The linear operating range is determined by performing series of staircase experiments as shown in Fig. 1. The input and output ranges for the linear region are indicated in Fig. 1, and are given in Eq. 1.

$$\begin{aligned} 0.1 \leq u_1 \leq 0.3, \quad 6.5 \leq u_2 \leq 7.5, \\ 82 \leq y_1 \leq 112, \quad 16 \leq y_2 \leq 18. \end{aligned} \tag{1}$$

The step responses of UCG are shown in Fig. 2, and it is found that there is no time delay between the input and output. The rise times and time constants determined by the step responses are summarized in Table 1.

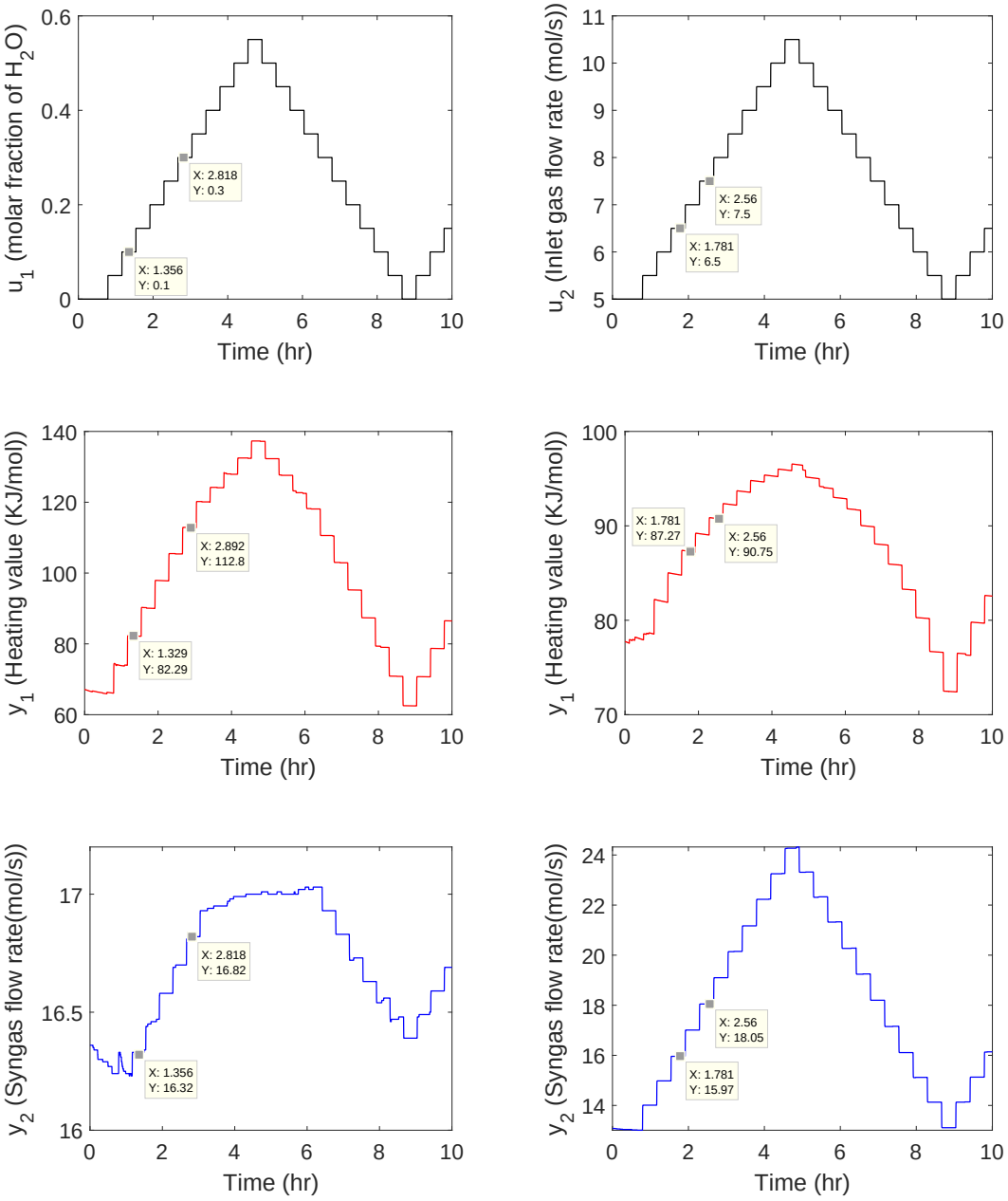

Figure 1: UCG response for staircase input

Table 1: Parameters obtained from step response

Inputs	**Outputs**	**Time constant** $\tau(s)$	**Rise time** $t_R(s)$
u_1	y_1	20.83	34.5
	y_2	19.03	31.1
u_2	y_1	20.03	30.3
	y_2	21.04	31.6

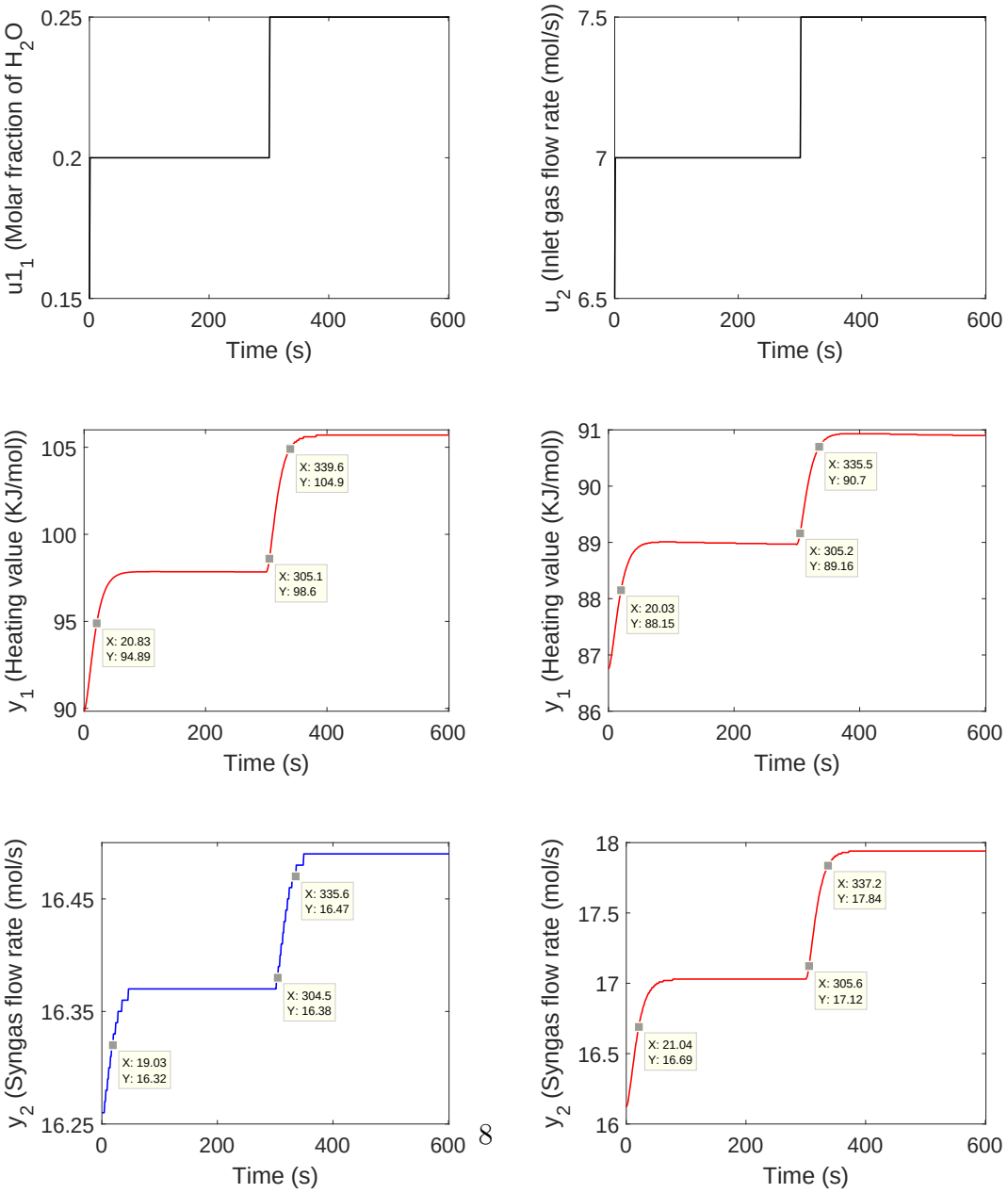

Figure 2: Step response of UCG

2.2. Model estimation and validation

After acquiring the certain characteristics of model, the subsequent step is to conduct an experiment for the model estimation and validation. The test input signal chosen for this experiment must satisfy the property of persistent excitation i.e. its bandwidth should cover the range of all frequencies of interest [33, 36, 37]. The perturbed signals such as step, random binary sequence (RBS), pseudo random binary sequence (PRBS), white noise, multisine and swept sin (chirp) are typically used for the identification of unknown systems. These excitation signals have flat power spectrum band within the user specified frequency band. In [38], authors have shown that the construction of advanced dedicated signals is a challenging task, and the most commonly used signals for system identification are step and PRBS signals.

In this work, PRBS signal has been used as an excitation signal and the design procedure is described in Table 2. A PRBS is a periodic signal, which switches in a certain fashion between two levels L_- and L_+, within a user specified frequency band. The bandwidth $[\omega_l \quad \omega_H]$ of input signal for multi-variable system is defined as

$$\omega_l = \frac{1}{\beta\tau_H} \leq \omega \leq \omega_H = \frac{\alpha}{\tau_l}, \tag{2}$$

where τ_H and τ_l are the highest and lowest time constants of the process, respectively, obtained from the step experiment; α is the ratio of open loop and desired closed loop time constants; $\beta\tau_H$ is the settling time of open loop system [36]. The number of shift registers (n_r) and the switching time T_{sw} are the important parameters to characterize the generated signal. The sequence repeats itself after $N_s T_{sw}$ units of time, where $N_s = 2^{n_r} - 1$. In [39] , authors have presented the guidelines to choose the switching and sampling time of PRBS and experiment length and given as

$$\frac{2.8\tau_l}{\alpha} \leq T_{sw} \leq \frac{2\pi\beta\tau_H}{N_s}, \tag{3}$$

$$N_s = 2^{n_r} - 1 \geq max\left(\frac{2\pi\beta\tau_H}{T_{sw}}, pD\right), \tag{4}$$

$$\text{where,} \quad D = \frac{5\tau_H}{T_{sw}},\ t_s = T_{sw}/4,$$

Table 2: Parameters obtained from step response

Parameters		**Values**
Lowest dominating time constant	$\tau_l(s)$	20.03
Highest dominating time constant	$\tau_H(s)$	21.04
Number of inputs	p	2
Closed-loop response parameter	α	2
Settling-time parameter	β	3
Switching time	$T_{sw}(s)^*$	27
Delay time	$D(s)^*$	3.8
Number of bits in PRBS sequence of length $N_s = 2^{n_r} - 1$	n^{r^*}	4

*Designed parameters, calculated from (3) and (4).

where p is the number of inputs, t_s is the sampling time and D is the delay time. In multiple-input, multiple-output (MIMO) system same PRBS can be used for all inputs provided that each input is delayed or shifted relative to the previous input by the delay time D in order to ensure that the input signals remain statistically uncorrelated. However, in this work separate PRBS is used for each input channel. The designed PRBS input signals having $T_{sw} = 27s$, $N_s = 15$ and maximum experiment length $N_s T_{sw} = 405$ samples, while the amplitude levels are defined on the basis of allowed linear operating range of each input.

CAVSIM is used to generate the essential input-output data required for system identification. After acquiring the input-output data sets, System Identification toolbox of Matlab is used to identify the linear state space model. The first 205 samples of input-output data sets are used for model estimation and remaining 200 samples are used for model validation. The outputs of nonlinear and linear models for each input and output are compared in Fig. 3 and it is found that the best fit results of each model g_{11}, g_{12} and g_{22} are 92.9%, 96.6% and 97.2% respectively. The residual analysis is an important part of system identification technique, which provides an insight about the model predictions [40]. It is essential that the residuals of each output must be uncorrelated with the past input signals in order to get better prediction results. In Fig. 3, it can be observed that the autocorrelation of residuals of each output and the cross-correlation between output residuals and each input lie within the confidence region. The system matrix of identified model is given in Eq. 5.

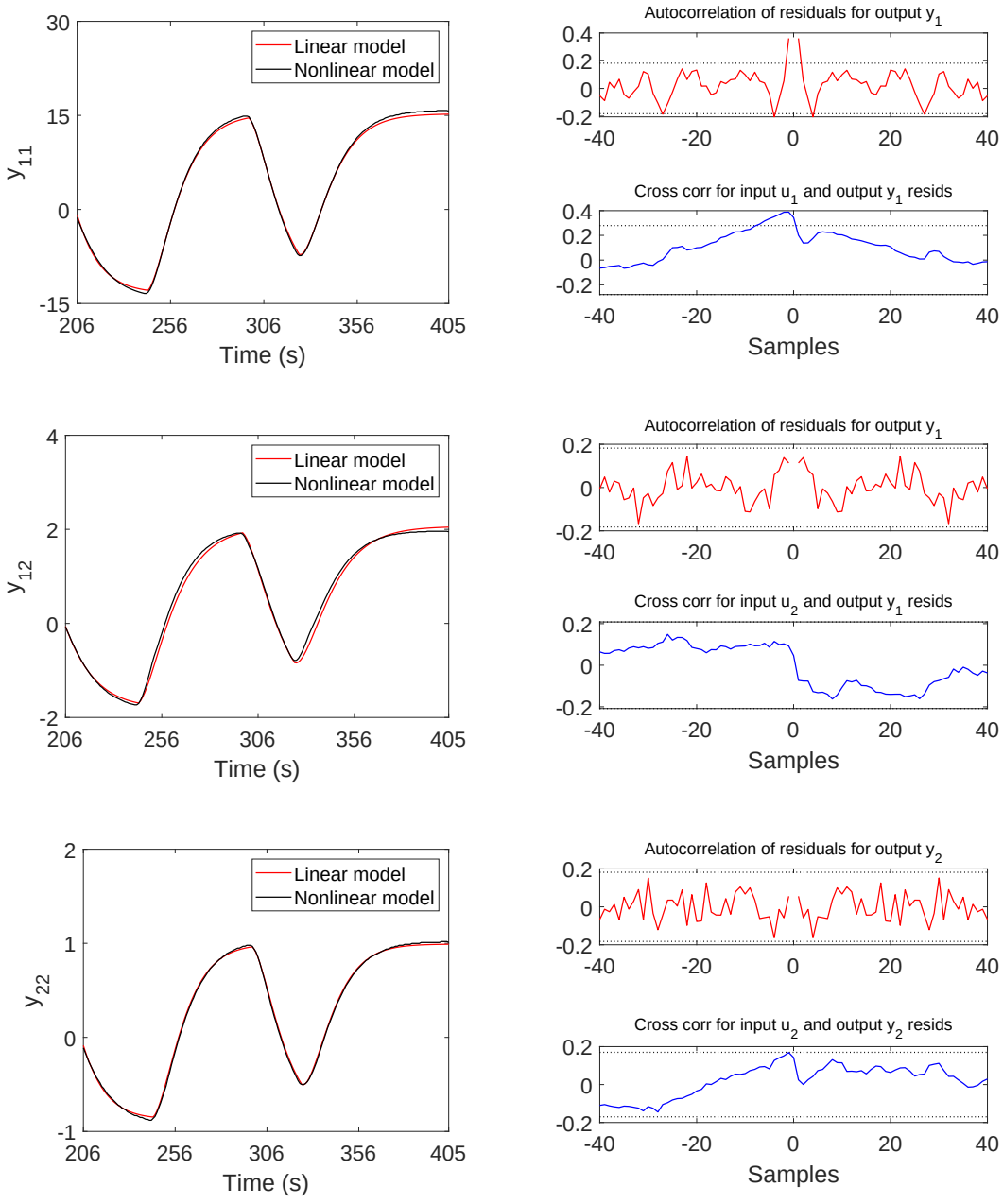

Figure 3: Comparison of linear and nonlinear models and residual analysis

$$\begin{bmatrix} y_1 \\ y_2 \end{bmatrix} = \begin{bmatrix} g_{11}(s) & g_{12}(s) \\ g_{21}(s) & g_{22}(s) \end{bmatrix} \begin{bmatrix} u_1 \\ u_2 \end{bmatrix}, \tag{5}$$

The transfer functions obtained from the state-space models are defined as

$$g_{11}(s) = \frac{1.799s + 1.458}{s^2 + 0.2s + 0.0102}, \qquad g_{12}(s) = \frac{0.04659s + 0.03473}{s^2 + 0.1915s + 0.008979},$$
$$g_{21}(s) = 0, \qquad g_{22}(s) = \frac{0.01951s + 0.0199}{s^2 + 0.1993s + 0.01071}.$$

where y_1, y_2 are the the outputs i.e. heating value (KJ/mol) and flow rate (mol/s) of syngas respectively. While u_1 (molar fraction of H_2O) and u_2 (inlet gas flow rate (mol/s)) represent the inputs of the system. It is found that the coupling lies in the UCG system as the heating value is sensitive to both the inputs. Thus, an H_∞ centralized control technique is employed to design the multi-variable robust controller for the UPT field, which is described in the subsequent section.

3. H_∞ controller design (S/KS mixed sensitivity)

In this section, the linear model in eq. 5 is employed to design a multi-variable H_∞ robust controller, which is insensitive to the model uncertainties. As the control objective is to maintain the two different physical quantities i.e. the flow rate and heating value of the syngas at the desired levels. Thus, the plant scaling is a preliminary step to be performed prior to the deign of controller, which is described in the subsequent section.

3.1. Preliminaries of H_∞ control design

Plant scaling has significant importance in the multi-variable systems which have different physical quantities. It helps the control engineer to make a decision about the desired performance of the system at the onset of controller design [41]. For this purpose, decision is made about the expected change in magnitudes of external signals like references, disturbance and measurement noise, and maximum allowed deviation of each input and output around the nominal point. The unscaled linear model of the UCG system is given in Eq. 6.

$$\tilde{y} = \tilde{G}\tilde{u} + \tilde{G}_{d_i}\tilde{d}_i, \quad \tilde{e} = \tilde{y} - \tilde{r}. \tag{6}$$

where $(\tilde{.})$ is used to represent the variables in their actual unscaled units. The scaling is performed by dividing each variable with its maximum allowed variation around the nominal point. Let $\tilde{u}_{j,max}$, $\tilde{d}_{i,max}$, $\tilde{r}_{k,max}$ and $\tilde{e}_{k,max}$ denote the maximum allowed change in input $\tilde{u}_j$, input disturbance $\tilde{d}_i$, reference $\tilde{r}_k$ and control error $\tilde{e}_k$. As the variables $\tilde{y}$, $\tilde{r}$ and $\tilde{e}$ have the same units, therefore, same scaling factor i.e. maximum control error $(\tilde{e}_{max})$ is applied to each variable. The unscaled and scaled quantities such as inputs, disturbances and control error are related by introducing the scaling matrices D_u, D_{d_i} and D_e, respectively.

$$\tilde{u} = D_u u, \quad \tilde{d}_i = D_{d_i} d_i, \quad \tilde{r} = D_e r, \quad \tilde{y} = D_e r. \tag{7}$$

The elements of scaling matrices given in Eq. 8 are determined from the staircase experiment of system identification, as described in section 2.

$$D_u = \begin{bmatrix} 0.1 & 0 \\ 0 & 0.5 \end{bmatrix}, \quad D_{d_i} = \begin{bmatrix} 0.1 & 0 \\ 0 & 0 \end{bmatrix}, \quad D_e = \begin{bmatrix} 15 & 0 \\ 0 & 1 \end{bmatrix}. \tag{8}$$

Introducing the scaled variables into Eq. 6 gives the scaled model, as given in Eq. 10.

$$G = D_e^{-1} \tilde{G} D_u, \quad G_{d_i} = D_e^{-1} \tilde{G}_{d_i} D_i, \tag{9}$$

$$y = Gu + G_{d_i} d_i, \quad e = y - r. \tag{10}$$

3.2. Problem formulation

The standard design structure of H_∞ robust controller is used to formulate the control problem, which is one of the most successful and reliable approach to design a linear robust controller [41]. The block diagram of closed loop system for UCG is shown in Fig. 4, which includes the UCG model, the elements of model uncertainty, feedback structure and controller, and performance specifications are incorporated by various weight functions. To model the effect of modeling inaccuracies due to linearization, an unstructured uncertainty–multiplicative input uncertainty is considered. The various sources of uncertainty in many practical applications are represented by the multiplicative input uncertainty because this type of uncertainty often occurs in real system and it also restricts the achievable performance [42]. The uncertain plant with an input multiplicative uncertainty is represented in Eq. 11.

$$\tilde{G}_(S) = G_{s_{nom}}(S)(I + W_\Delta \Delta); \ \|\Delta\|_\infty \leq 1, \tag{11}$$

where $\tilde{G}_(S)$ and $G_{s_{nom}}(S)$ represent the perturbed and nominal models, respectively. The unmodeled and neglected dynamics are represented by a complex perturbation Δ and the multiplicative weight W_Δ is a diagonal matrix of stable minimum phase transfer functions used to normalize the uncertainties to be less than unity.

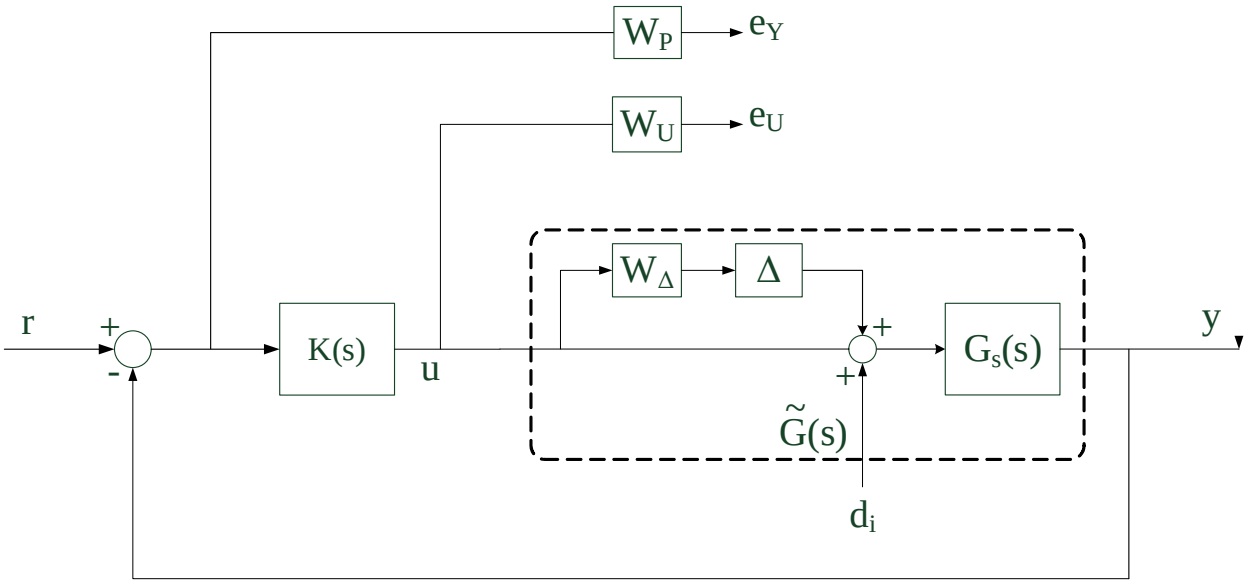

Figure 4: Block diagram of closed-loop system with performance specifications

The H_∞ controller for the UCG system is designed by incorporating the generalized plant ($\tilde{P}$) or interconnected system, controller (K) and the uncertainty block (Δ) into the standard configuration of H_∞ controller as shown in Fig. 5. The control and all exogenous input signals like reference inputs (r) and an input disturbance (d_i) are represented by u and a vector w, respectively. The steam flow rate is considered as an input disturbance for the system. While the control effort (e_U) and tracking error (e_Y) to be penalized are considered as exogenous outputs and denoted by a vector z. The measurable quantities such as syngas heating value (y_1) and flow rate (y_2) are represented by a vector y. The generalized plant ($\tilde{P}$) and the nominal system ($\tilde{N}$) in which K is absorbed into the interconnection structure are given below.

$$w = \begin{bmatrix} r & d_i \end{bmatrix}^T,\ z = \begin{bmatrix} e_Y & e_U \end{bmatrix}^T,\ v = r - y.$$

$$\tilde{P} = \begin{bmatrix} W_P I & -W_P G_s & -W_P G_s \\ 0 & 0 & W_U I \\ -I & -G_s & -G_s \end{bmatrix}. \tag{12}$$

where

$$\tilde{P}_{11} = \begin{bmatrix} W_P I & -W_P G_s \\ 0 & 0 \\ -I & 0 \end{bmatrix},\ \tilde{P}_{12} = \begin{bmatrix} -W_P G_s \\ W_U I \\ -G_s \end{bmatrix},\ \tilde{P}_{21} = \begin{bmatrix} -I & -G_s \end{bmatrix},\ \tilde{P}_{22} = \begin{bmatrix} -G_s \end{bmatrix}.$$

$$\tilde{N} = \tilde{F}_l(\tilde{P}, K) \triangleq \tilde{P}_{11} + \tilde{P}_{12} K (I - \tilde{P}_{22} K)^{-1} \tilde{P}_{21}. \tag{13}$$

where $\tilde{F}_l(\tilde{P}, K)$ is the lower linear fractional transformation of $\tilde{P}$ and K.

$$\tilde{N} = \begin{bmatrix} W_P(I - T_o) & W_P G_s (T_o - I) \\ W_U K S_o & -W_U K G_s S_o \end{bmatrix}. \tag{14}$$

Similarly,

$$\tilde{F} = \tilde{F}_u(\tilde{N}, \Delta) \triangleq \tilde{N}_{22} + \tilde{N}_{21} \Delta (I - \tilde{N}_{11} \Delta)^{-1} \tilde{N}_{12} \tag{15}$$

where $\tilde{F}_u(\tilde{N}, \Delta)$ is the upper linear fractional transformation of $\tilde{N}$ and Δ. The closed loop transfer function matrix $\Phi(s)$ from w to z is given in Eq. 16. The H_∞ norm of $\Phi(s)$ must be less than unity for all possible stable perturbations to attain the performance objectives.

$$\begin{bmatrix} e_Y \\ e_U \end{bmatrix} = \begin{bmatrix} W_p S_o & W_p \tilde{G} S_i \\ W_u S_i K & -W_u K S_o \tilde{G} \end{bmatrix} \begin{bmatrix} r \\ d_i \end{bmatrix}. \tag{16}$$

or

$$\begin{bmatrix} e_Y \\ e_U \end{bmatrix} = \Phi(s) \begin{bmatrix} r \\ d_i \end{bmatrix}.$$

where $S_o = (I + \tilde{G}K)^{-1}$ and $S_i = (I + K\tilde{G})^{-1}$ are the output and input sensitivity functions, respectively.

3.2.1. Robust stability and performance constraints

The $M\Delta$ and $\tilde{N}\Delta$ configurations shown in Fig. 6a and Fig. 6b are used to perform the robust stability and performance analysis of an uncertain system, respectively. It is essential to satisfy that the nominal stability (NS) condition i.e. $\tilde{N}$ is internally stable prior to carrying out the robust stability (RS), nominal performance (NP) and robust performance (RP) analysis. When $\tilde{N}$ is stable then it can be seen in Eq. 15 that the instability may only occur due to the feedback term $(I - \tilde{N}_{11\Delta})^{-1}$. Therefore, if the system has nominal stability then the stability of $\tilde{N}\Delta$ and $M\Delta$ structures become equivalent to each other. The stability objectives are formulated as:

$$NS \Leftrightarrow \tilde{N} \text{is internally stable.} \tag{17a}$$

$$\begin{aligned} RS &\Leftrightarrow \|M = \tilde{N}_{11}\|_\infty < 1, \forall\omega, \text{NS and } \Delta \text{ is stable} \\ &\Leftrightarrow \|W_U K(I + GK)^{-1}\|_\infty < 1, \forall\omega, \text{NS and } \Delta \text{ is stable.} \end{aligned} \tag{17b}$$

The robust performance analysis of an uncertain system is performed by computing structured singular value (μ) [41]. The standard configuration for μ analysis is shown in Fig. 6, and its simplest form is defined by Eq. 18

$$\mu(\tilde{M})^{-1} \triangleq \min_{\Delta}\{\bar{\sigma}(\Delta) | det(I - \tilde{M}\Delta) = 0 \text{ for structured } \Delta\}. \tag{18}$$

where $\Delta = \text{diag}\Delta_i$ represents a set of complex matrices with a given block diagonal structure in which few blocks may be restricted to be real, and some of them may be repeated. The transfer function from the output to the input of the uncertainties is represented by a complex matrix $\tilde{M} = \tilde{N}_{11}$, $det()$ is the determinant, and $\bar{\sigma}()$ is the maximum singular value. The definition of μ given in Eq. 18 considers varying $\bar{\sigma}(\Delta)$, however, it is preferred to normalize Δ such that $\bar{\sigma}(\Delta) \leq 1$. It can be done by scaling Δ by a factor β , and find the smallest β at which the matrix $I - \beta\tilde{M}$ becomes singular, and it gives $\mu = 1/\beta$. The real non-negative function $\mu(\tilde{M})$, called the structured singular value, is defined by

$$\mu(\tilde{M}) \triangleq \frac{1}{min\{\beta | det(I - \tilde{M}\Delta) = 0 \text{ for structured } \Delta,\ \bar{\sigma}(\Delta) \leq 1\}}. \tag{19}$$

The μ is a measure of smallest possible perturbation which can make the system unstable. When $\mu = 1$, this implies that the perturbation exists in

the system having $\bar{\sigma}(\Delta) = 1$ is large enough to make it unstable ($I - \tilde{M}\Delta$ becomes singular). Thus, the smaller value of μ is desired i.e. $\mu(\tilde{M}) \leq 1$ in the designing of robust controller to attain more robustness in the presence of large uncertainty.

The conditions of nominal and robust performance are given in Eq. 20 , which are obtained by using the standard $\tilde{N}\Delta$ configuration

$$NP \Leftrightarrow \|\tilde{N}_{22}\|_\infty < 1 \Leftrightarrow \|W_P G_s\|_\infty < 1, \text{and NS.} \tag{20a}$$

$$RP \Leftrightarrow \|\tilde{F}\|_\infty = \|\tilde{F}_u(\tilde{N}, \Delta)\|_\infty < 1, \forall \|\Delta\|_\infty \leq 1 \tag{20b}$$

$$\Leftrightarrow \mu_{\tilde{\Delta}}(\tilde{N}) < 1, \forall \omega, \tilde{\Delta} = \begin{bmatrix} \Delta & 0 \\ 0 & \Delta_P \end{bmatrix}, \text{and NS.}$$

where Δ is a block diagonal matrix and the detailed structure is described by the represented uncertainty, and $\tilde{\Delta}$ is used to indicate the H_∞ performance objectives and it is always a full complex matrix.

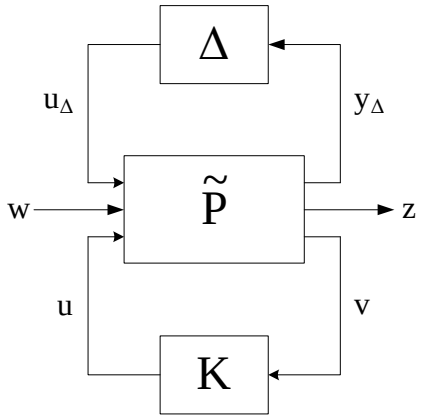

Figure 5: General configuration for controller synthesis

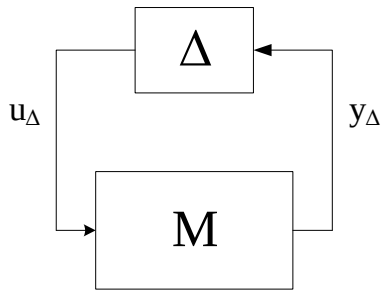

(a) $M\Delta$-structure for robust stability analysis

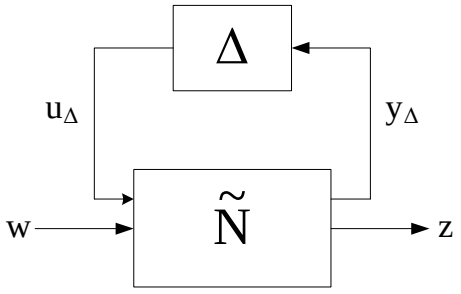

(b) $\tilde{N}\Delta$-structure for robust performance analysis

Figure 6: General configurations for controller analysis

3.2.2. Selection of weights

The performance objectives to minimize the tracking error and control effort are closely related to the sensitivity function S. The magnitude of S must be small at the frequency ranges where the small tracking error is required in each of the controlled output. Thus, it can be achieved by introducing an integrator s^{-1} in the weights related with each controlled output. In well posed standard H_∞ control problem, the use of only pure integrator in performance weight is not suitable in a sense that the generalized plant $\tilde{P}$ could not be stabilized by the feedback controller K. Thus, the typical specifications for S in frequency domain are determined in terms of peak sensitivity (M_s) and bandwidth ω_b.

$$|S(s)| = \left| \frac{s}{s/M_b + \omega_b} \right|, \ s = j\omega, \ \forall\omega. \tag{21}$$

Or equivalently,

$$|W_P S| \leq 1, \tag{22}$$

where,

$$W_P = \frac{s/M_b + \omega_b}{s}. \tag{23}$$

The weight function given in Eq. 23 is modified by introducing the maximum steady-state tracking error (ϵ) i.e. $|S(0)| \leq \epsilon$, which satisfies $W_P(0) \leq 1/\epsilon$ such that $|W_P S|_\infty \leq 1$

$$W_P = \frac{s/M_b + \omega_b}{s + \omega_b \epsilon}. \tag{24}$$

The parameters ω_b, ϵ and M_b have correlation with the closed loop band width, steady state error and overshoot, respectively. The values of $\omega_b = 0.001rad/s$, $M_b = 1.5$ and $\epsilon = 10^{-4}$ are chosen in the proposed problem. For simplicity equal weights are used for both channels. The weight W_U is taken as $0.5I_{2\times 2}$ at all frequencies to avoid saturation on the control input.

$$w_{P_{ii}} = \frac{0.6667s + 0.001}{s + 1e - 07},\ i = 1, 2. \tag{25}$$

$$W_P = \begin{bmatrix} w_{P_{11}} & 0 \\ 0 & w_{P_{22}} \end{bmatrix}. \tag{26}$$

A simple stable, minimum phase transfer function shown in Eq. 27 is used to normalize the multiplicative uncertainty.

$$w_{\Delta_{ii}} = \frac{\alpha s + r_o}{\alpha/r_\infty s + 1}, \tag{27}$$

where r_o, r_∞ is the relative uncertainty at steady state and higher frequencies, respectively. The relative uncertainty reaches 100% is approximately shown by $1/\alpha$. In the proposed problem similar uncertainty weights are used for both inputs, having $\alpha = 0.1$, $r_o = 0.2$ and $r_\infty = 3$.

$$w_{\Delta_{ii}} = \frac{0.1s + 0.2}{\frac{0.1}{3}s + 1},\ i = 1, 2. \tag{28}$$

$$W_\Delta = \begin{bmatrix} w_{\Delta_{11}} & 0 \\ 0 & w_{\Delta_{22}} \end{bmatrix}. \tag{29}$$

3.3. Results and discussion

The Matlab robust control toolbox is used to determine the H_∞-optimal controller by employing S/KS mixed sensitivity design method. The controller is synthesized by ignoring the uncertainties and only the nominal plant is considered in controller design. The infinity norm of $F_l(P_{nominal}, K)$ is minimized with respect to K by the S/KS mixed sensitivity controller. While in the given problem $F_l(P_{nominal}, K)$ is the closed loop transfer matrix ($\Phi(s)$) represented in Eq. 17. The desired performance specifications are incorporated by the performance weight matrix W_P and the inverse of performance weight matrix defines the upper bound on $|S|$. The desired bandwidth and upper bound on $|S|$ at different frequency ranges is shown by the frequency

response of inverse performance weight matrix in Fig. 7. It can be seen that the $1/|W_P|$ is equal to unity at the frequency $\omega_b = 0.001rad/s$, which is the desired bandwidth. While it has magnitude equal to $A = 1e^{-4}$ and $M = 1.4$ at low and high frequencies, respectively.

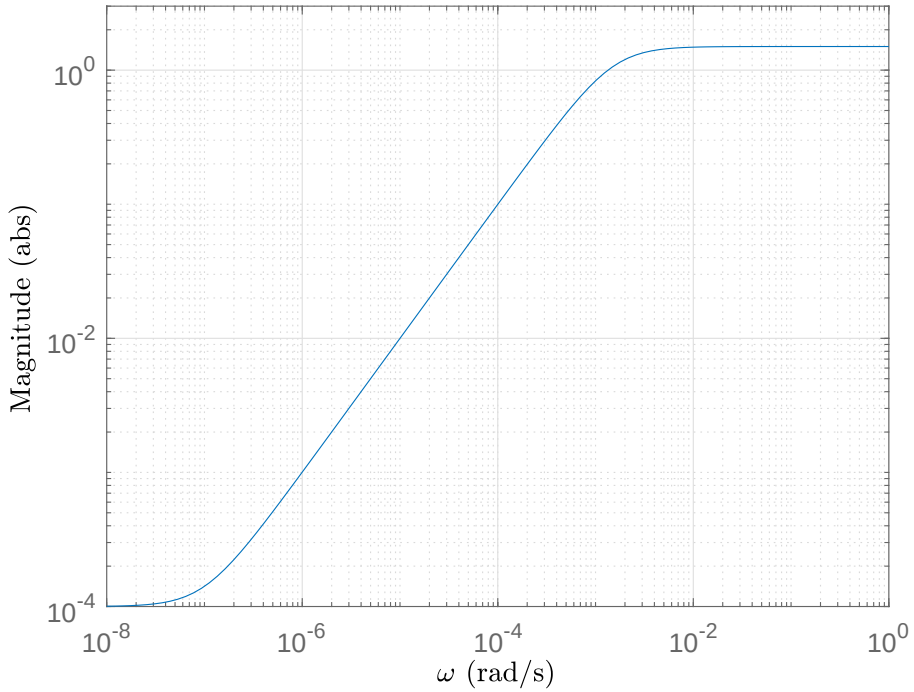

Figure 7: Inverse of performance weight

The singular-value plots of S, KS and T for the perturbed plant are shown in Fig. 8a, 8b and 8c, respectively. It can be seen that the magnitude of S is lower than the upper bound and the magnitude of T at low frequencies is unity, which conform that the desired performance is achieved. While the singular-values of KS are lower than their upper bounds, which shows that the actuators are not saturated to attain the desired bandwidth. The nominal stability properties of closed-loop transfer functions are same due to the similar internal dynamics. Thus, these results also show that the closed-loop system has achieved the nominal stability. Moreover, the effect of output sensitivity $S_{out} = y/d_i$ to disturbance for perturbed plant is also analyzed in Fig. 8d . It can be seen that disturbance has negligible effect at

low frequencies, which means that the closed-loop system is not susceptible to disturbance over that frequency range.

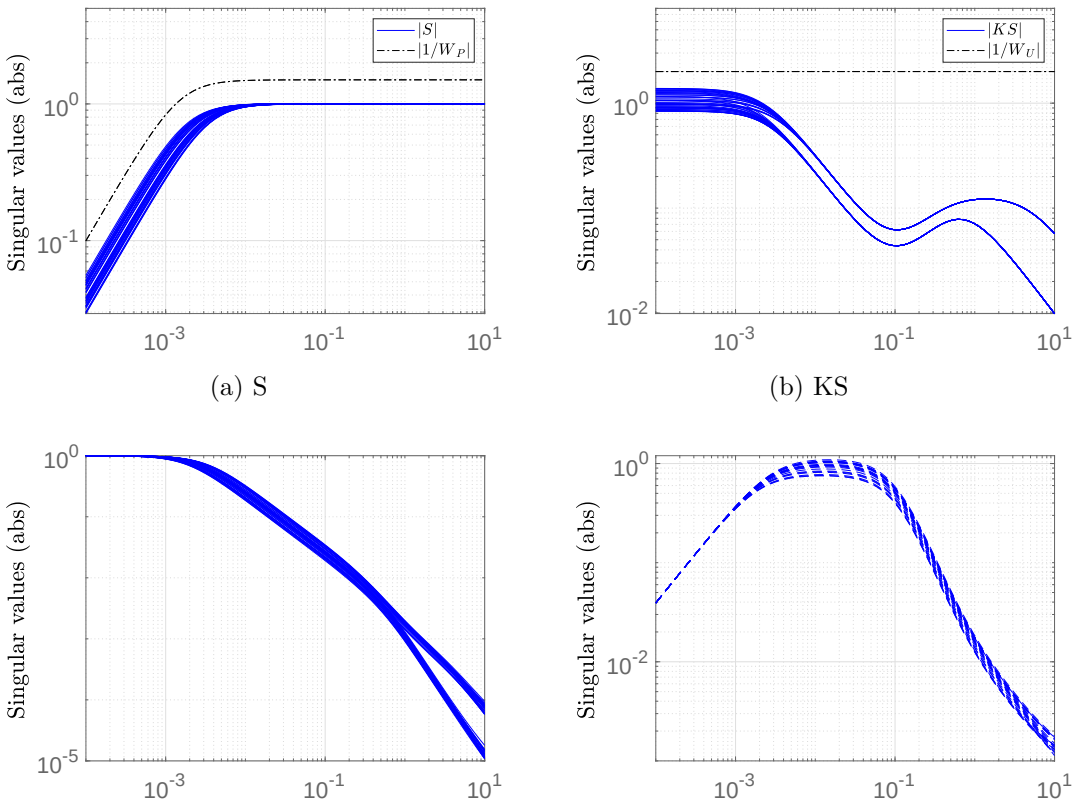

(a) S (b) KS

(c) T (d) Output sensitivity to disturbance

Figure 8: Frequency response of closed-loop system

The robust stability and nominal performance of the closed-loop system are determined by plotting the singular values of M and $\tilde{N}_{22}$, as shown in Fig. 9 The singular values can be seen to be less than unity, which shows that the closed loop system meets the robust stability and nominal performance constraints. The closed-loop system can tolerate up to 503% of the modeled uncertainty, as given in Table 3. In Fig. 10, the frequency response of μ is shown to analyze the robust performance of closed-loop system. The controller has achieved the robust performance as μ is less than unity. The performance margins in the form of upper and lower bound are given in Table 4. Moreover, it is observed that the model uncertainty of 115% can lead

to input/output gain of 0.871 at 0.00014 rad/seconds.

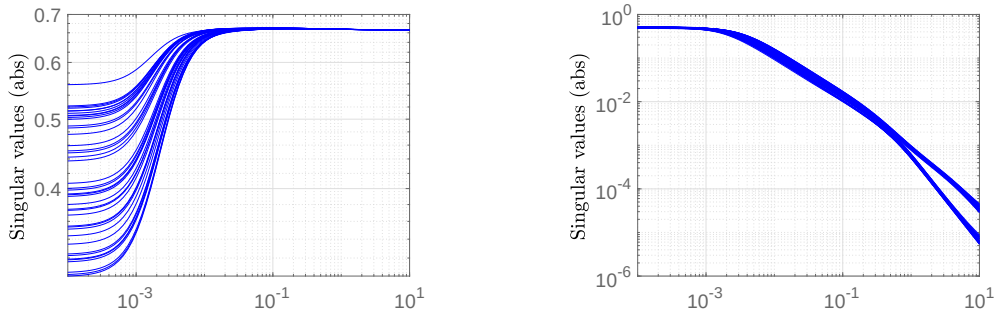

(a) (b)

Figure 9: (a) Robust stability, (b) Nominal performance

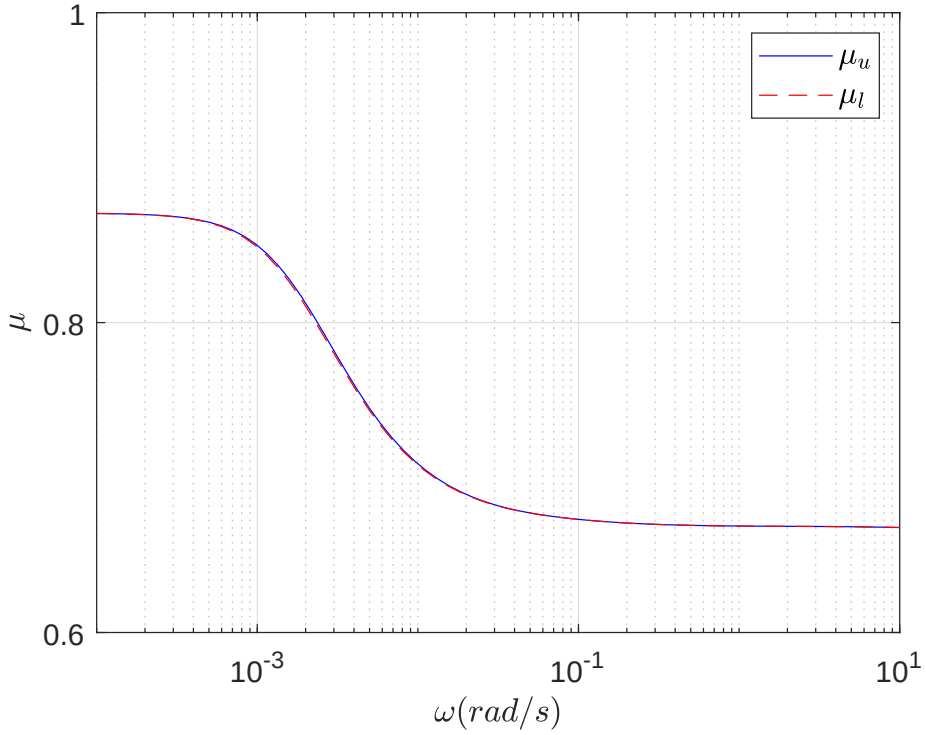

Figure 10: Robust performance analysis

Table 3: Robust stability margins for H_∞ controllers

Controller	**Order**	**Stability margins**		
		Lower bound $(1/\mu_u)$	Upper bound $(1/\mu_l)$	Destabilizing frequency (rad/s)
S/KSl	7	5.296878	5.296881	0.001

Table 4: Robust performance margins for H_∞ controllers

Controller	**Order**	**Performance margins**		
		Lower bound $(1/\mu_u)$	Upper bound $(1/\mu_l)$	Destabilizing frequency (rad/s)
S/KSl	7	1.1475	1.1478	0.00013

The closed-loop step response of linear system is shown in Fig. 11 The step signal is applied at all exogenous inputs and it can be seen that both the outputs track the desired response in the presence of model uncertainty and input disturbance. In addition, it also meets the desired performance specifications corresponding to the transient characteristics, such as the overshoot, time constant and settling time. The input disturbance is introduced to the framework to assess the controller's success in rejecting the disruption. The optimal amount of water is one of the important parameter for the successful operation of UCG rector. The excess water can disrupt the operation of UCG gasifier and reduces its temperature due to the endothermicity of the steam gasification reaction. Therefore, an optimal level of H_2O is necessary for the successful operation of UCG field [9]. Thus, the water influx from the surrounding strata acts as an input disturbance in the UCG process, as it increases the molar fraction of steam in UCG rector. In Fig. 12, it can be seen that the controller caters the input disturbance by manipulating the molar fraction of steam and maintains an optimum value of steam.

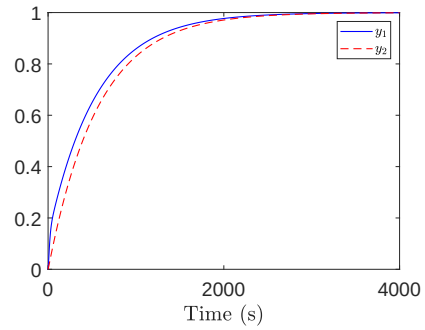

(a) Step response (Step in r_1, r_2, d_i)

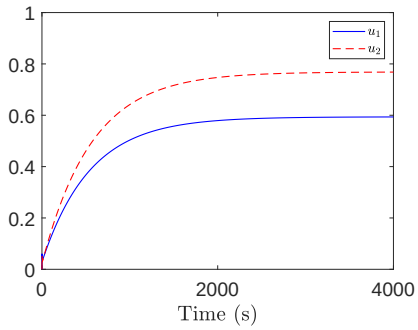

(b) Control effort for tracking

Figure 11: Closed-loop transient response of scaled-linear system

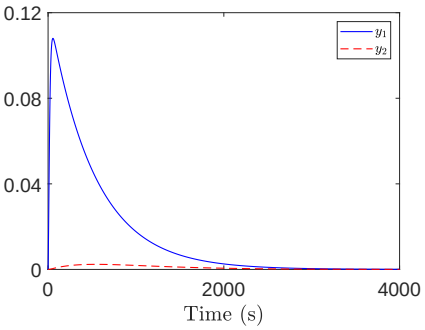

(a) Input disturbance step response

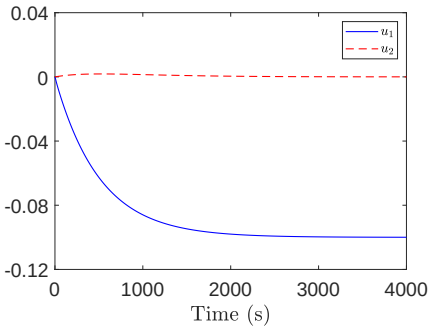

(b) Control effort to reject d_i

Figure 12: Closed-loop response to input disturbance

4. Implementation of Controller on Actual Model

The robust controller designed on the basis of linear model in section 3 is discretized and implemented on the actual nonlinear model i.e. CAVSIM in order to assess the robustness of the controller. Moreover, the dynamics of control valve and the gas analyzer are modeled with the following transfer functions [24].

$$G_1(s) = \frac{e^{-\tau_{d_c} s}}{\tau_c s + 1}, \quad G_2(s) = \frac{e^{-\tau_{d_g} s}}{\tau_g s + 1} \tag{30}$$

It has been experimentally found that the control valve and gas analyzer have negligible time delays (τ_{d_c}, τ_{d_g}) and are therefore ignored in Eq. 30.

While the time constants for the control valve (τ_c) and gas analyzer (τ_g) were found to be about $10s$. The controller implementation scheme on actual system is shown in Fig. 13. It is pertinent to mention that the controller has been designed from a scaled model, therefore, it is essential to include the scaling matrices D_u, D_e and D_{d_i} in the actual implementation. Moreover, the nominal operating points of inputs are included after the inputs scaling matrix in such a way that the inputs feed to CAVSIM are the actual inputs. While in order to create the scaled inputs to the controller, the nominal operating points of outputs are subtracted from the actual outputs of CAVSIM prior to output scaling matrix and feedback.

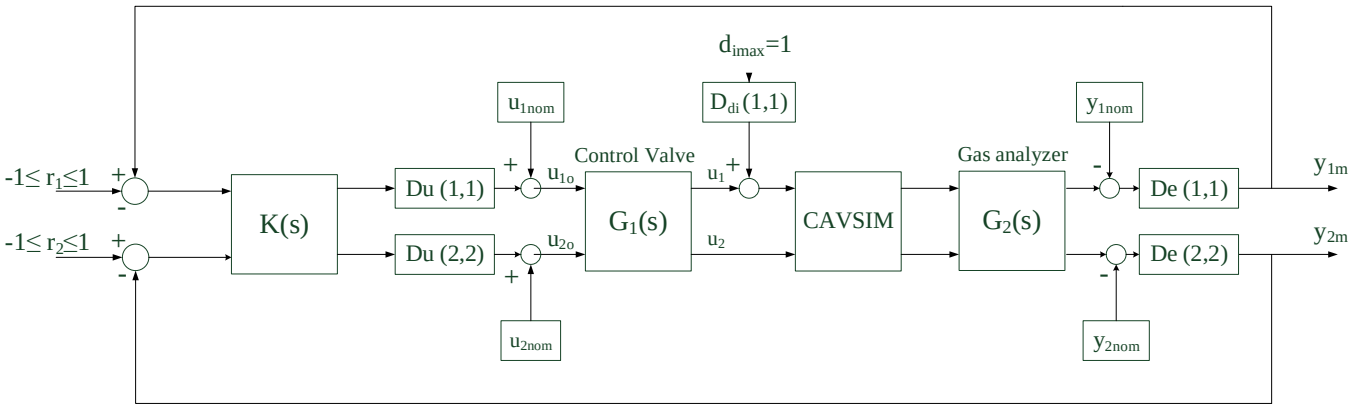

Figure 13: Controller implementation scheme

The UCG process is operated in open loop with the nominal inputs for 06 hours and the closed loop process starts afterwards. Fig. 14 shows that the controller effectively hold both the outputs to their desired levels by adjusting the control inputs as well as maintaining the control efforts within the allowed range, as given in Eq. 1. The desired trajectory of outputs are chosen in such a way that they cover the entire range of operating points for which the controller has been designed. As described earlier in section 3.3, the molar fraction of steam is an input disturbance in the UCG process, and it is shown in Fig. 15b where the disturbance enters the system at 8^{th} hour. It can be seen that the controller rejects the input disturbance by varying the inlet molar fraction of H_2O. When the water influx increases the molar fraction of H_2O, the controller maintains the optimal amount of H_2O by reducing the amount of inlet steam.

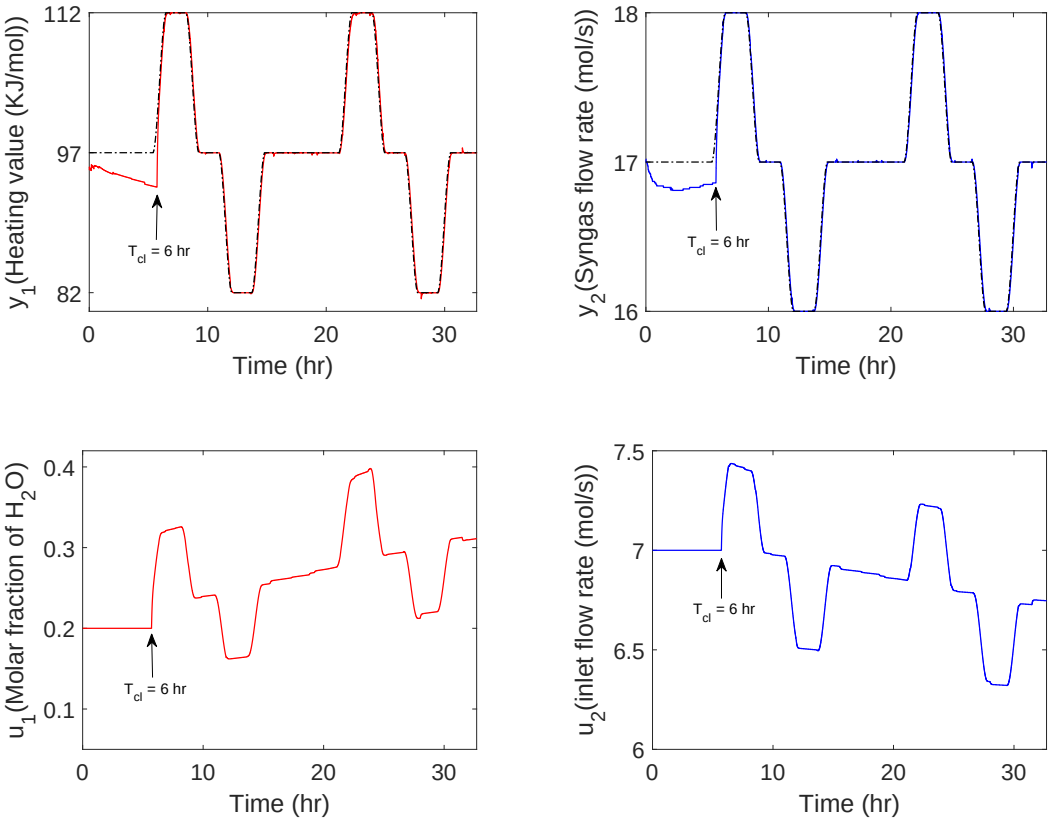

Figure 14: Closed-loop response of nonlinear model to the reference inputs

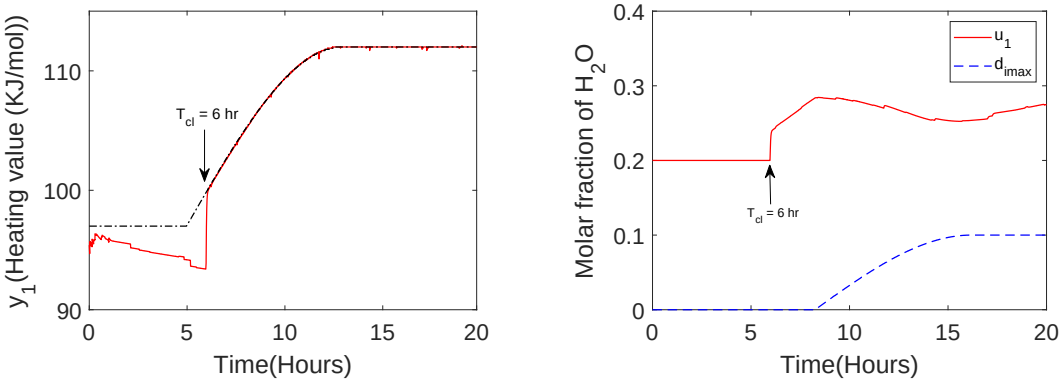

(a) Output (b) Control effort and disturbance profile

Figure 15: Close-loop response of nonlinear model to the input disturbance

5. Conclusion

In this article, the significance of multi-variable based closed loop system for UCG is highlighted. It has been shown that the energy per unit time of a UCG site can be improved by developing a multi-variable control system. Due to the complexity of actual UCG model, a simple linear multi-variable model has been identified to design a robust controller for the UPT field. An H_∞-optimal controller is designed using S/KS method and the control problem is formulated by using standard H_∞ control configuration. The robust stability and performance analysis have been performed in the presence of model uncertainty. Moreover, it is shown that the linear closed loop system meets all the desired transient requirements in the presence of input disturbance and modeling uncertainties. Finally, the robustness of controller has been assessed by implementing it on CAVSIM, and it is shown that the outputs attain their desired values in the presence of an input disturbance and modeling inaccuracies.

In future, a more accurate nonlinear model will be identified by employing an advanced nonlinear system identification technique. Moreover, the designed controller will be implemented at the UPT field in order to achieve the desired level of energy per unit time.

References

[1] N. V. Gnanapragasam, B. V. Reddy, M. A. Rosen, Hydrogen production from coal gasification for effective downstream co2 capture, International Journal of Hydrogen Energy 35 (10) (2010) 4933–4943.

[2] G. Perkins, Underground coal gasification–part i: Field demonstrations and process performance, Progress in Energy and Combustion Science 67 (2018) 158–187.

[3] G. Perkins, Underground coal gasification–part ii: Fundamental phenomena and modeling, Progress in Energy and Combustion Science 67 (2018) 234–274.

[4] R. Sathre, L. Gustavsson, N. Le Truong, Climate effects of electricity production fuelled by coal, forest slash and municipal solid waste with and without carbon capture, Energy 122 (2017) 711–723.

[5] A. W. Bhutto, A. A. Bazmi, G. Zahedi, Underground coal gasification: From fundamentals to applications, Progress in Energy and Combustion Science 39 (1) (2013) 189–214.

[6] L. Yang, J. Liang, L. Yu, Clean coal technology-study on the pilot project experiment of underground coal gasification, Energy 28 (14) (2003) 1445–1460.

[7] M. Imran, D. Kumar, N. Kumar, A. Qayyum, A. Saeed, M. S. Bhatti, Environmental concerns of underground coal gasification, Renewable and Sustainable Energy Reviews 31 (2014) 600–610.

[8] G. Perkins, Mathematical modeling of underground coal gasification, Ph.D. thesis, PhD Thesis: School of Materials Science & Engineering, Faculty of Science … (2005).

[9] A. A. Uppal, Modeling and control of underground coal gasification, Ph.D. thesis, COMSATS Institute of Information Technology, Islamabad, Pakistan (2016).

[10] V. Prabu, S. Jayanti, Laboratory scale studies on simulated underground coal gasification of high ash coals for carbon-neutral power generation, Energy 46 (1) (2012) 351–358.

[11] Y. Cui, J. Liang, Z. Wang, X. Zhang, C. Fan, D. Liang, X. Wang, Forward and reverse combustion gasification of coal with production of high-quality syngas in a simulated pilot system for in situ gasification, Applied Energy 131 (2014) 9–19.

[12] S. J. Friedmann, R. Upadhye, F.-M. Kong, Prospects for underground coal gasification in carbon-constrained world, Energy Procedia 1 (1) (2009) 4551–4557.

[13] G. o. S. Sindh Coal & Energy Department, Thar coal fields technical specification, block-v, `http://www.sindhcoal.gos.pk/coal-fields/thar-coalfield/` (2012).

[14] A. Arshad, A. I. Bhatti, R. Samar, Q. Ahmed, E. Aamir, Model development of ucg and calorific value maintenance via sliding mode control, in: 2012 International Conference on Emerging Technologies, IEEE, 2012, pp. 1–6.

[15] A. A. Uppal, A. I. Bhatti, E. Aamir, R. Samar, S. A. Khan, Control oriented modeling and optimization of one dimensional packed bed model of underground coal gasification, Journal of Process Control 24 (1) (2014) 269–277.

[16] G. Samdani, P. Aghalayam, A. Ganesh, S. Mahajani, A process model for underground coal gasification–part-iii: Parametric studies and ucg process performance, Fuel 234 (2018) 392–405.

[17] K. Kostúr, J. Kacur, Development of control and monitoring system of ucg by promotic, in: 2011 12th international carpathian control conference (ICCC), IEEE, 2011, pp. 215–219.

[18] K. Kostúr, J. Kačúr, The monitoring and control of underground coal gasification in laboratory conditions, Acta Montanistica Slovaca 13 (1) (2008) 111–117.

[19] K. J. Åström, T. Hägglund, PID controllers: theory, design, and tuning, Vol. 2, Instrument society of America Research Triangle Park, NC, 1995.

[20] K. Kostúr, J. Kačur, Extremum seeking control of carbon monoxide concentration in underground coal gasification, IFAC-PapersOnLine 50 (1) (2017) 13772–13777.

[21] A. M. Chaudhry, A. Arshad Uppal, Y. M. Alsmadi, A. I. Bhatti, V. I. Utkin, Robust multi-objective control design for underground coal gasification energy conversion process, International Journal of Control (2018) 1–8.

[22] A. Fossard, T. Floquet, Introduction: an overview of classical sliding mode control, in: Sliding mode control in engineering, CRC Press, 2002, pp. 22–49.

[23] A. A. Uppal, A. I. Bhatti, E. Aamir, R. Samar, S. A. Khan, Optimization and control of one dimensional packed bed model of underground coal gasification, Journal of Process Control 35 (2015) 11–20.

[24] A. A. Uppal, Y. M. Alsmadi, V. I. Utkin, A. I. Bhatti, S. A. Khan, Sliding mode control of underground coal gasification energy conversion process, IEEE Transactions on Control Systems Technology.

[25] A. A. Uppal, S. S. Butt, A. I. Bhatti, H. Aschemann, Integral sliding mode control and gain-scheduled modified utkin observer for an underground coal gasification energy conversion process, in: 2018 23rd International Conference on Methods & Models in Automation & Robotics (MMAR), IEEE, 2018, pp. 357–362.

[26] A. A. Uppal, S. S. Butt, Q. Khan, H. Aschemann, Robust tracking of the heating value in an underground coal gasification process using dynamic integral sliding mode control and a gain-scheduled modified utkin observer, Journal of Process Control 73 (2019) 113–122.

[27] G. Samdani, P. Aghalayam, A. Ganesh, R. Sapru, B. Lohar, S. Mahajani, A process model for underground coal gasification–part-ii growth of outflow channel, Fuel 181 (2016) 587–599.

[28] G. Samdani, P. Aghalayam, A. Ganesh, R. Sapru, B. Lohar, S. Mahajani, A process model for underground coal gasification–part-i: Cavity growth, Fuel 181 (2016) 690–703.

[29] S. B. Javed, A. A. Uppal, A. I. Bhatti, R. Samar, Prediction and parametric analysis of cavity growth for the underground coal gasification project thar, Energy 172 (2019) 1277–1290.

[30] C. Thorsness, J. Britten, Lawrence livermore national laboratory underground coal gasification project:final report, Tech. rep., Lawrence Livermore National Laboratory, CA (USA), UCID-21853 (1989).

[31] D. W. Camp, A review of underground coal gasification research and development in the united states, Tech. rep., Lawrence Livermore National Lab.(LLNL), Livermore, CA (United States) (2017).

[32] T. C. Britten, J.A., Cavsim user manual, Lawrence Livermore National Laboratory report. UCID-21667 (1989).

[33] L. Ljung, System identification: Theory for the user (book style).

[34] H. Hjalmarsson, System identification of complex and structured systems, European journal of control 15 (3-4) (2009) 275–310.

[35] S. Gaikwad, D. Rivera, Control-relevant input signal design for multivariable system identification: Application to high-purity distillation, in: IFAC World Congress, Vol. 349, Citeseer, 1996.

[36] R. Ghosh, et al., Input designs for identification of ill-conditioned multivariable systems.

[37] A. I. Bhatti, Advanced sliding mode controllers for industrial applications, Ph.D. thesis, Engineering (1998).

[38] R. Pintelon, J. Schoukens, System identification: a frequency domain approach, John Wiley & Sons, 2012.

[39] D. Rivera, S. Gaikwad, X. Chen, Control-id: A demonstration prototype for control-relevant identification, in: Proceedings of 1994 American Control Conference-ACC'94, Vol. 2, IEEE, 1994, pp. 2055–2059.

[40] R. P. Pothukuchi, J. Torrellas, A guide to design mimo controllers for architectures (2016).

[41] S. Skogestad, I. Postlethwaite, Multivariable feedback control: analysis and design, Vol. 2, Wiley New York, 2007.

[42] S. Ghabraei, H. Moradi, G. Vossoughi, Design & application of adaptive variable structure & h∞ robust optimal schemes in nonlinear control of boiler-turbine unit in the presence of various uncertainties, Energy 142 (2018) 1040–1056.